Transparent Light-Driven Hydrogel Actuator Based on Photothermal Marangoni Effect and Buoyancy Flow for Three-Dimensional Motion

Deng Pan, Dong Wu,* Peng-Ju Li, Sheng-Yun Ji, Xuan Nie, Sheng-Ying Fan, Guo-Yang Chen, Chen-Chu Zhang, Chen Xin, Bing Xu, SuWan Zhu, Ze Cai, YanLei Hu, JiaWen Li,* and JiaRu Chu

Marangoni-effect-driven actuators (MDAs) have the advantages of direct light-to-work conversion and convenient operation, which makes it widely researched in the cutting-edge fields including robots, micromachines, and intelligent systems. However, the MDA relies on the surface tension difference and it only works on the 2D liquid–air interface. Besides, the MDAs are normally pure black due to the light-absorption material limitation. Herein, a transparent light-driven 3D movable actuator (LTMA) and a 3D manipulation strategy are proposed. The LTMA is composed of photothermal nanoparticles-doped temperature-responsive hydrogel, whose surface energy changes as the nanoparticles absorb light energy. The 3D manipulation strategy combines Marangoni effect with photothermal buoyancy flow for realizing complex self-propellant and floating/sinking motions. The LTMA can perform more advanced tasks such as 3D obstacle avoidance and 3D sampling. Benefiting from the porous structure of hydrogel, LTMA can naturally absorb the chemical molecules for remote sampling and automated drug delivery. The light-driven, transparent, three-dimensionally movable, and programmable actuator has promising prospects in the field of micromachines and intelligent systems.

1. Introduction

Light-driven actuators can convert light energy into mechanical work and realize movements such as bending, rotation, translation, sinking, and floating, which makes them widely used in the field of robots, micromachines, and intelligent systems.[1] Compared with other driving methods including heat, electricity, humidity, pneumatic expansion, and magnetic, the light-driven strategy is advantageous because it does not require complex equipment and can be remotely controlled in a noncontact manner.[2,3] Moreover, light is a clean, safe, and sustainable energy source and its parameters (intensity, polarization, wavelength, and repetition frequency) can be precisely adjusted.[4] To realize the light-driven movements of an actuators, researchers have proposed several light-driven manipulation methods based on different mechanisms including optical tweezers, photochemical effects, photoelectric conversion, and photothermal effects.[5] Optical tweezers utilize the force of light momentum to manipulate and capture nano/microparticles, but the force is too small to manipulate large objects. The photochemical-effect-driven actuators are usually based on some specific photoresponsive chemical materials such as azobenzene or spiropyran derivatives that can change their molecular properties under the light stimulus, but this method suffers from relatively small deformation. The photoelectric-conversion-driven actuators can realize high-speed propulsion and rotation motions by absorbing light energy and emitting energetic electrons, but this method needs a harsh vacuum environment to perform the photoelectric conversion. Among these light-driven strategies, the photothermal-driven actuators based on light-induced heat have the distinct advantages of simple design principles, controllable reconfigurations, and outstanding performance.

Photothermal-driven strategies can be classified into two categories. One of the photothermal strategies relies on the periodic deformation caused by light-induced heat. For example, Jiang et al. used the grapheme nanoplatelets-doped

D. Pan, Prof. D. Wu, P.-J. Li, Dr. S.-Y. Ji, S.-Y. Fan, G.-Y. Chen, C. Xin, Dr. B. Xu, Dr. S. Zhu, Dr. Z. Cai, Dr. Y. Hu, Dr. J. Li, Prof. J. Chu
Hefei National Laboratory for Physical Sciences at the Microscale
CAS Key Laboratory of Mechanical Behavior and Design of Materials
Department of Precision Machinery and Precision Instrumentation
University of Science and Technology of China
Hefei, Anhui 230027, P. R. China
E-mail: dongwu@ustc.edu.cn; jwl@ustc.edu.cn
X. Nie
Department of Polymer Science and Engineering
University of Science and Technology of China
Hefei, Anhui 230026, P. R. China
Dr. C.-C. Zhang
Anhui Province Key Lab of Aerospace Structural Parts Forming
Technology and Equipment
Institute of Industry and Equipment Technology
Hefei University of Technology
Hefei, Anhui 230009, P. R. China

polydimethylsiloxane (PDMS) as the light-absorbing deformation material to constitute actuators that can float, bend, and swim to a preset location.[2,6] However, the high temperature (usually >100 °C) caused by the photothermal effect weakens the safety and durability of actuators. Another light-driven strategy relies on the Marangoni effect that has the advantages of directly realizing the light-to-work conversion.[7–9] The Marangoni effect drives actuators by the liquid surface tension difference because the liquid with high surface tension will pull on the surrounding liquid with low surface tension spontaneously.[10] Therefore, as long as the surface tension gradient is produced at the desired position through the photothermal effect, the driving force can be effectively generated for driving the actuators. Based on this mechanism, considerable research efforts have been devoted for realizing the motions of actuators. For example, Okawa et al. combined a PDMS block and the vertically aligned carbon nanotube forests to make the light-driven actuator. The carbon nanotube can absorb light energy and generate surface tension gradients so that this actuator can realize the linear and rotational motions under the drive of photothermal surface tension.[9] Maggi et al. developed asymmetric microgears around which the surface tension gradients generated a nonzero total torque, leading to efficient conversion of light energy into rotational motion.[11] Zhang et al. used femtosecond laser to treat the PDMS surface into a black photothermal layer with superhydrophobicity, making the PDMS block float on the water surface and be driven by the photothermal effect.[12] Liao et al. enhanced the actuating speed by utilizing aligned thermally conducting 1D multiwalled carbon nanotubes that can generate a localized surface tension gradient for high spatial resolution propulsion.[7]

However, the Marangoni effect occurs only at the 2D liquid–liquid or liquid–air interface, and the marangoni effect driven actuators (MDA) can only float on liquids, limiting its further application. Furthermore, due to the material limitations, the previous MDAs are pure black. The black actuators will limit its application such as optical detection, optical communication, and optical camouflage. Until now, transparent light-driven actuators based on the Marangoni effect that can realize the 3D motions both on liquid and under liquid have not yet been developed.

In this work, we report a transparent light-driven 3D movable actuator (LTMA) that can perform not only programmable self-propellant but also floating–sinking motions under the control of the near-infrared (NIR) laser beam or sunlight. The LTMA is composed of a temperature-responsive hydrogel (pNIPAM) and photothermal nanoparticles (CuS nanoparticles). The surface energy of pNIPAM changes as the CuS nanoparticles absorb the light energy and convert it into thermal energy. As a result, the self-propellants of LTMA can be realized based on the surface tension difference. Besides, inspired by the buoyancy flow in nature that is caused by liquid temperature and concentration changes,[13] the porous hydrogel can sink by absorbing liquid molecules, and then float by using the NIR laser beam to heat up the LTMA and subsequently generate the buoyant flow around it. The floating/sinking ability based on the buoyancy flow is not limited by the liquid depth. Due to the lower critical solution temperature (LCST = 32 °C) of the pNIPAM,[6,14] the 3D manipulations of the LTMA require low input energy, which means it can be operated under the irradiation of the low power NIR laser or the sunlight. The thickness of LTMA is only 100 μm and the concentration of photothermal nanoparticles is low (0.001–0.006 mg mL^{-1}), which enable the LTMA transparent. To the best of our knowledge, it is the first time that the hydrogel is used to prepare a transparent actuator that is able to move three-dimensionally based on the photothermal Marangoni effect and photothermal buoyancy flow.

2. Results and Discussion

2.1. The Fabrication of Transparent Light-Driven Actuators

Intelligent hydrogels, which can respond to external stimulation including temperature, pH, and light, have been widely used in the field of biosensors, drug delivery, and smart actuators due to their unique responsibility and biocompatibility. Thermal-stimuli-responsive hydrogels are the most widely used polymer system because the temperature is easy to control. The material used in this work is composed of a thermal-stimuli-responsive hydrogel (pNIPAM) and photothermal nanoparticles (CuS). The pNIPAM is a kind of widely used thermal-stimuli-responsive hydrogel whose surface energy changes as the temperature changes,[15] and it can be fabricated by the UV light or IR femtoseconds beam[16] and the reason for choosing CuS nanoparticles as the photothermal material is that their preparation does not require expensive equipment. A typical movement process of LTMA under the light drive is shown in **Figure 1**a,b. First, as the laser is irradiated on the LTMA, the photothermal nanoparticles convert the laser energy into heat and generate buoyant flow around it, causing the LTMA floating. After floating onto the liquid–air interface, the LTMA was heated unevenly by the laser beam that caused the temperature and surface energy difference between two sides of LTMA. As a result, the LTMA can move controllably under the light drive. Finally, when the LTMA arrives at the preset position, and the LTMA without the laser irradiation sinks naturally by absorbing the surrounding liquid molecules. The LTMA is a hydrogel film formed by UV exposing the homemade hydrogel and CuS nanoparticles mixture, and the preparation process is shown in Figure S1, Supporting Information. The nanoparticles and hydrogel formed stable dispersion systems by magnetic stirring and ultrasonic mixing. The thickness of hydrogel mixture was controlled as about 100 μm by spin coating. A UV exposure system consisting of a DMD and a 4× long working distance objective lens (Figure 1c) was used to expose the hydrogel to a predesigned shape such as panda, fish, and Chinese character (Figure 1d–f). Finally, the hydrogel film was transferred into ethanol to remove the unprocessed area and release the transparent LTMA. As a demonstration of transparence, the fish-like LTMA is placed on the photo and the colors and graphics below LTMA can be clearly seen, proving that the LTMA has good optical transparent characteristics (Figure 1g). Besides, the transparency can be adjusted by controlling the concentration of CuS nanoparticles. As the volume ratio of CuS/pNIPAM increase from 1:6 to 6:6 (Experimental Section, Preparation of the LTMA), the LTMA becomes more opaque (Figure 1h) and absorbs more light energy with wavelengths above 750 nm (Figure 1i).[17] It is worth noting that the conventional MDA are
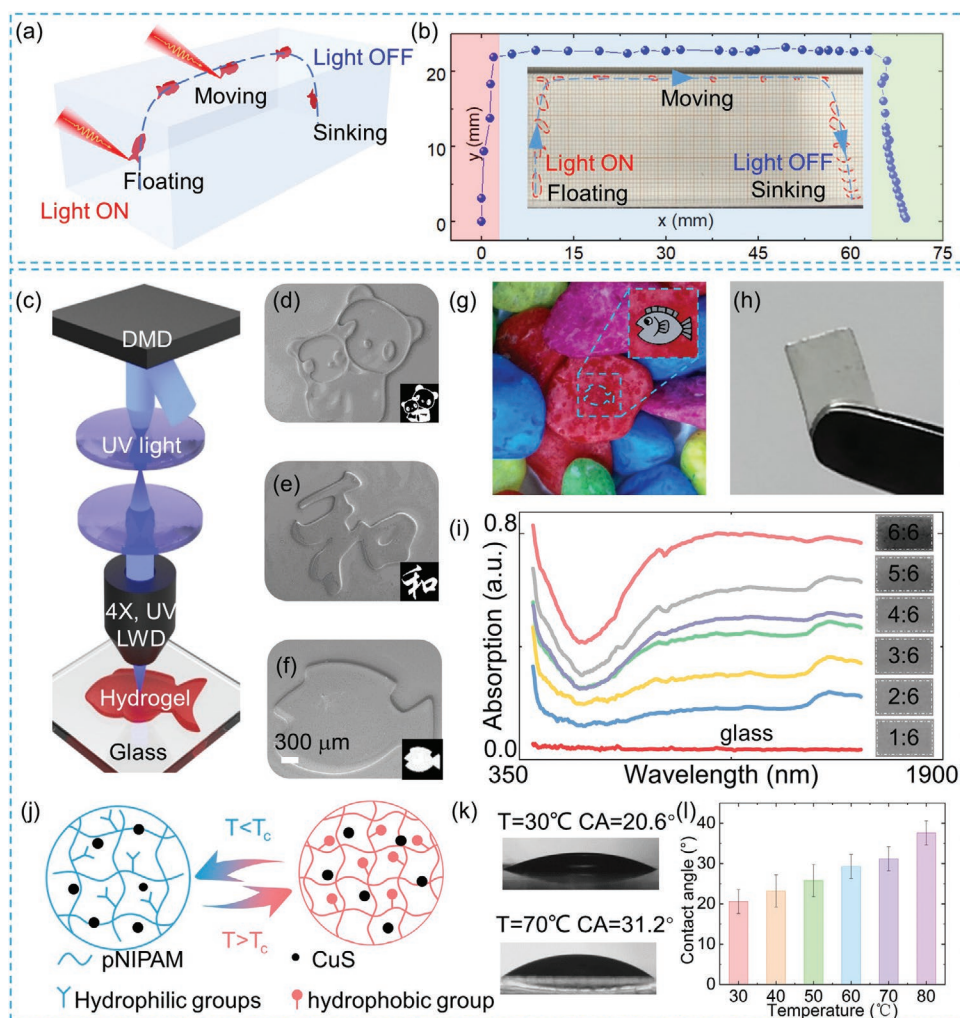
Figure 1. The processing, characterization, and movement of LTMA. a) The schematic diagram of LTMA moving process, which consists of floating, moving, and sinking movement. b) The coordinates of LTMA in a typical moving process. c) The fabrication system of LTMA that consists of a UV light, DMD, 4f system, 4× long working distance objective lens, and a 3D platform. d–f) The UV system can fabricate the LTMA to arbitrary patterns, such as panda, fish, and Chinese character. g,h) The optical images of LTMA film, scale bar 5 mm. i) The UV–vis–NIR spectra of LTMA under different nanoparticle concentrations. The inset photographs are LTMA films with different nanoparticle concentrations, and the ratio refers to the volume ratio of CuS nanoparticle solution to pNIPAM hydrogel. The volume ratio of 1:6, 2:6, 3:6, 4:6, 5:6, and 6:6 correspond to CuS nanoparticles concentration of 0.001035, 0.00207, 0.003105, 0.00414, 0.005175, and 0.00621 mg mL^{-1}, respectively. j) The polymer chains inside pNIPAM have hydrophobic and hydrophilic domains below and above the LCST. k) The CA of LTMA–ethanol is 31.2° and 20.6° when the temperature is 70 and 30 °C, respectively. l) The CA of LTMA–ethanol will increase as the temperature increase.

pure black. This is because the conventional actuators contain a large amount of light-absorbing materials to generate a high temperature difference for obtaining an enough Marangoni driving force, which leads the actuators to be pure black and limits its further applications. Herein, the LTMA is transparent for two reasons. On the one hand, the main material of LTMA is pNIPAM that is transparent, and a thinner film of 100 μm thickness further improves the transparency. On the other hand, the pNIPAM can make a significant surface energy difference with small temperature differences because the LSTC of pNIPAM is only 32 °C, which means that LTMA does not need to contain a large number of photothermal particles. The polymer chains inside pNIPAM have hydrophobic and hydrophilic domains below and above the LCST, which means that the contact angle (CA) changes along with the change of

pNIPAM temperature (Figure 1j,k).[18] Figure 1l shows the dynamic CAs of pNIPAM–ethanol, from which we can see that the CA in higher temperature is larger than that in lower temperature.

2.2. The Floating and Sinking Process of LTMA

The floating and sinking process of LTMA in ethanol is shown in **Figure 2**a, and the relationship between height and time are shown in Figure 2b. After 5.5 s laser irradiation, the LTMA started to float up, and it reached liquid–air interface at 8.5 s. Once the LTMA reached the liquid–air interface, it would float on the liquid surface steadily and not sink under the action of surface tension because the LTMA repelled the liquid molecules
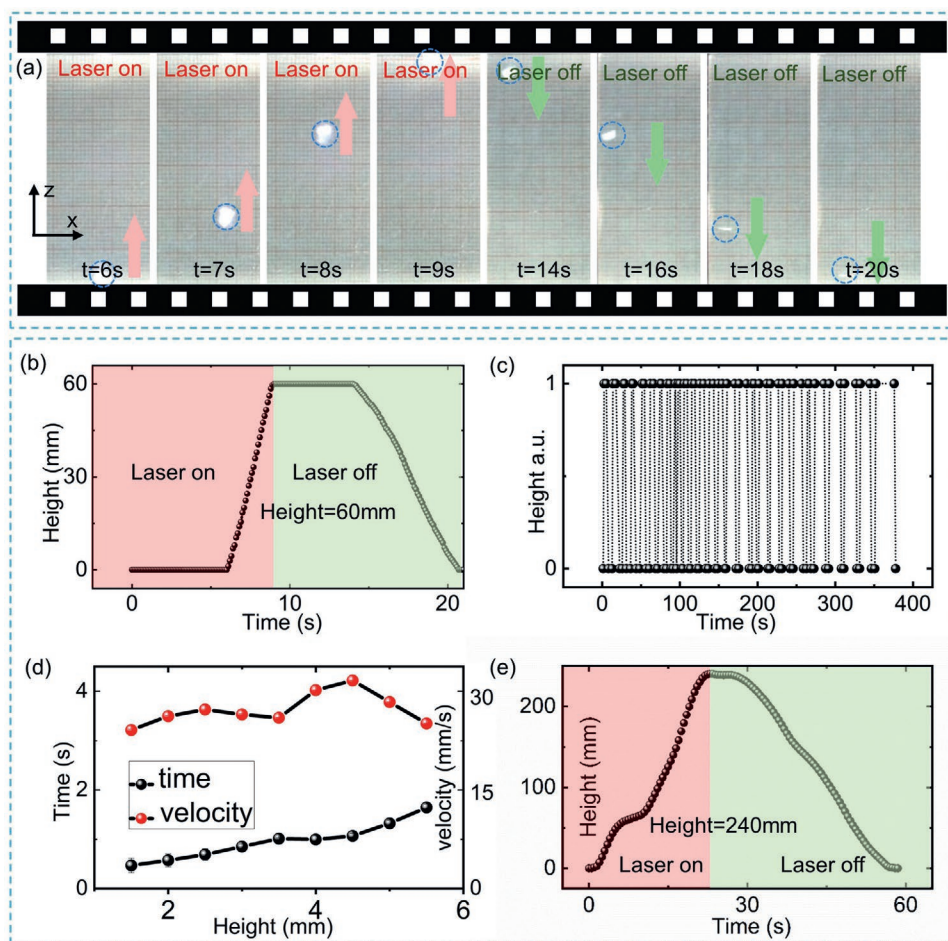
ADVANCED
SCIENCE NEWS
www.advancedsciencenews.com

ADVANCED
FUNCTIONAL
MATERIALS
www.afm-journal.de

Figure 2. The process that LTMA moves up and down. a) LTMA moves up when the laser is on and moves down when the laser is off. b) The height changes when LTMA is floating and sinking. c) The floating speed stays constant when the depth of liquid changes. d) The time that LTMA moves from the bottom to the top of liquid increase as the depth of liquid increase. e) The change of height with time under 50 floating-and-sinking cycles.

under the laser-induced heating. However, when the laser was turned off, the LTMA cooled down and gradually absorbed liquid molecules, sinking into the bottom under the action of gravity. Therefore, the controllable floating and sinking motions can be realized by heating up and cooling down the LTMA. The liquid used in this work is ethanol because ethanol can easily penetrate LTMA, which leads to a rapid sinking process. Besides, the LTMA can float and sink in many organic solutions such as *n*-propanol, isopropanol, and acetone. The floating–sinking cycles can be repeated for many times (Video S2, Supporting Information, and Figure 2c). It is worth noting that the floating is not limited by depth. As shown in Figure 2d, as the liquid depth changes from 10 to 50 mm, the floating speed is constant at about 38 mm s⁻¹. As a demonstration, an experiment was conducted in a 240 mm deep ethanol whose depth was 24 000 times of the thickness of the LTMA (Video S1, Supporting Information). After 30 s of laser irradiation, LTMA floated up to the liquid–air interface successfully (Figure 2e). The LTMA has the characteristics of controllable and repeatable floating–sinking ability that is not limited by the liquid depth, providing the possibility of remote and cordless control.

2.3. The Mechanism of LTMA Floating under the Light Drive

The reason why LTMA can float in the liquid is that it converts the light energy into heat and generates a buoyancy flow around it. In nature, temperature and concentration affect the density of the flowing fluid resulting in buoyancy. Similarly, there was also buoyancy flow around the LTMA due to the temperature difference between LTMA and the surrounding liquid environment. We use the $\rho_0 g_p (T - T_0)$ to describe the temperature-related force that causes the fluid flow and convective heat transfer, in turn affecting temperature distribution, where ρ_0 is the fluid density, α_p is the coefficient of volumetric thermal expansion, T is the temperature of LTMA, and T_0 is the temperature of the surrounding environment. According to the law of conservation of heat, we have

$$\rho_0 C_p \upsilon \cdot \nabla T - \nabla \cdot \left(k \nabla T \right) = 0 \tag{1}$$

where k denotes the thermal conductivity, υ is the fluid velocity, and c_p is the specific heat capacity of the fluid. Besides, based
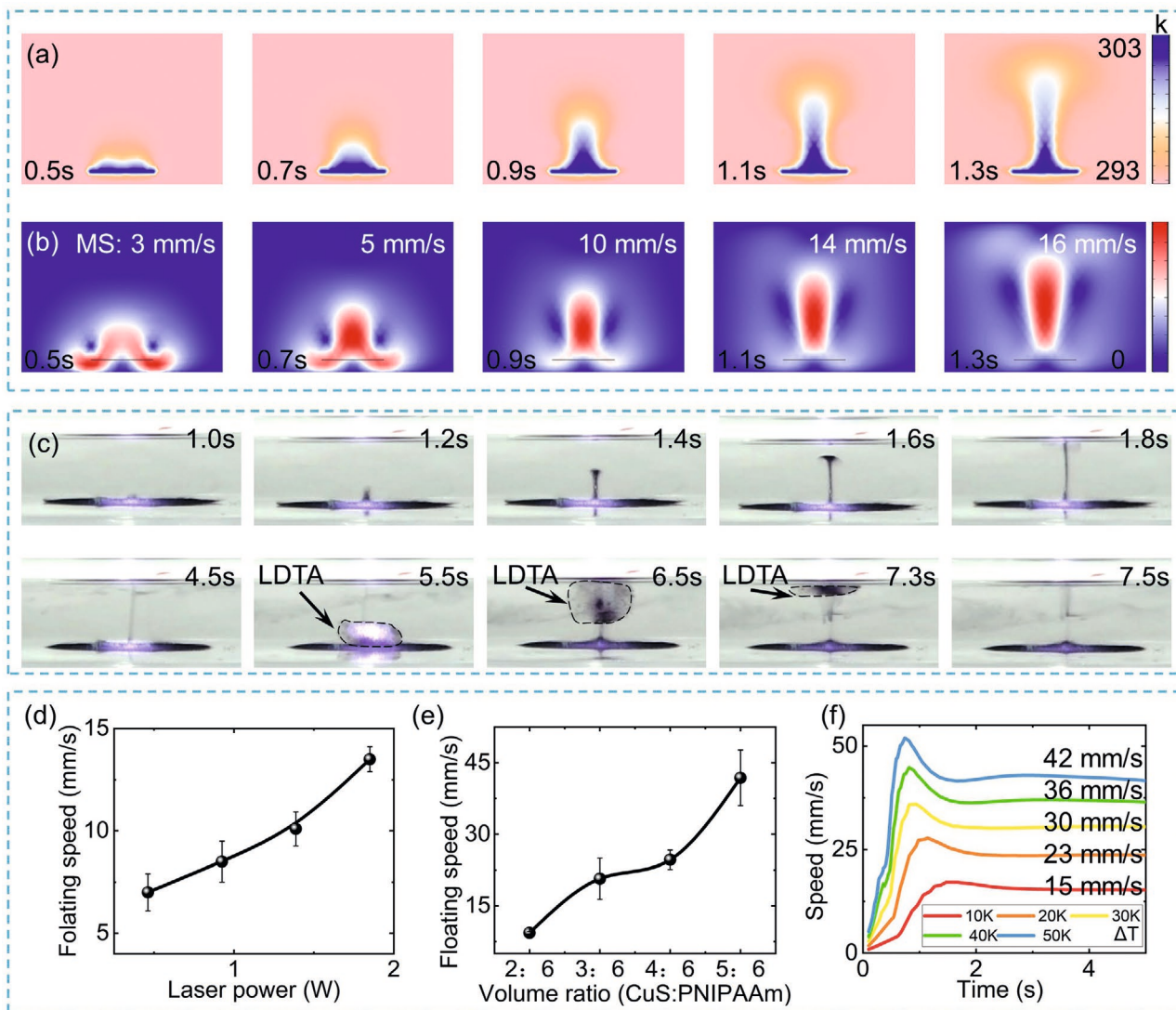
Figure 3. Simulation and experimental results of LTMA rising under buoyancy flow. a) Simulation results of temperature distribution at different times when the initial temperature difference is set to be 20 K. b) Simulation results of flow velocity distribution at different times when the initial temperature difference is set to be 20 K. c) The experimental results that a buoyancy flow generates as LTMA is heating up and the LTMA moves from the bottom to the top of liquid under the action of liquid flow. d) The floating speed under different laser power. e) The floating speed under different nanoparticle concentrations. f) Simulation results of maximum flow velocity at different times under different temperature difference.

on the Navier–Stokes equations, the relationship between the fluid velocity v and temperature can be written as

$$\rho_0 \left(\frac{\partial v}{\partial t} + v \cdot \nabla v \right) = -\nabla p + \nabla \cdot \mu \left(\nabla v + (\nabla v)^T \right) + \rho_0 g \alpha_p (T - T_0) \quad (2)$$

where p is the fluid pressure and μ is the dynamic viscosity. Here, in order to analyze the dynamic process of buoyancy flow, the finite element simulation software was used to calculate the flow velocity and temperature distribution at different times based on the Equations (1) and (2). Besides, an experiment was conducted to confirm our hypothesis. First, as the laser turned on, the LTMA absorbed the laser energy and changed the temperature distribution around. When the temperature difference (ΔT) is set to 10 K, the temperature

distribution and floating velocity distribution at different times are shown in **Figure 3**a,b, respectively. At 0.5 s, the high-temperature and high-floating-speed zone mainly concentrated near the LTMA. As the liquid density decreased with increasing temperature, the liquid flowed upwards causing a buoyancy flow. Then, the buoyant flow rose to the top of the liquid surface during 0.8 s, and the max floating speed (MS) increased from 3 to 16 mm s^{-1} (Figure 3d,e). The experimental results are consistent with the simulation results (Videos S3 and S4, Supporting Information). In order to clearly show the buoyant flow, a drop of blue ink was dropped on LTMA in advance. The buoyant flow occurred after the laser irradiated the sample for 1 s. At 1.8 s, the buoyant flow reached the top of the liquid surface. The time of the buoyant flow from bottom to top is 0.8 s and the floating speed is 15 mm s^{-1},

which are exactly consistent with the simulation results. Then, the LTMA was driven to float up under the action of the flowing liquid. The LTMA started to rise at 5.3 s and reached the top of the liquid surface at 7.3 s (Figure 3c). Furthermore, according to Navier–Stokes equations, when the laser power is greater or the nanoparticle concentration is higher, the LTMA will rise faster due to more light energy absorption and faster flow velocity (Figures S3 and S4a,b, Supporting Information). In order to further validate it, we characterize their floating speeds at different laser power and nanoparticle concentrations (Figure 3d,e). As the laser power increased from 0.5 to 2 W, the surface temperature increased from 31.4 to 64.1 °C (Figure S2, Supporting Information) and the floating speed increased from 7 to 13.5 mm s^{-1} with the CuS nanoparticles concentration of 0.003 mg mL^{-1}. As the CuS nanoparticles concentration increased from 0.002 to 0.005 mg mL^{-1}, the floating speed increased from 8 to 43 mm s^{-1} with the laser power of 2 W. The experimental floating speed is the same order of magnitude as the simulation results, as shown in Figure 3f, Figure S4c,d, Supporting Information. When the temperature difference increases from 10 to 50 K, the theoretical flow speed increases from 13 to 42 mm s^{-1}. Besides, the speed of LTMA can be flexibly adjusted by the laser energy and the CuS concentration, because the flow speed can be controlled by the temperature difference. In order to clarify the driving effect of buoyant flow, we fabricated LTMA with thickness varying from 50 to 225 µm (Figure S5, Supporting Information). The laser power intensity was set to be 1 W cm^{-2}, and the driving effects were shown in Table S1, Supporting Information. When the thickness of LTMA is smaller than 150 µm, the buoyancy flow can successfully bring the LTMA to the top of ethanol. When the thickness of LTMA is between 125 and 200 µm, the lift force of the buoyant flow can only flip the LTMA. Finally, as the thickness of LTMA is further increased to more than 200 µm, buoyant flow cannot make LTMA move. The possible reason is that the floating of LTMA is the result of the counterbalance between the lift force of the buoyant flow and the gravity of LTMA. When the lift force is greater than the gravity, the LTMA can reach the liquid surface successfully. When the lift force is slightly greater than the gravity, the LTMA will flip. When the lift force is less than the gravity, the LTMA will not be able to move. In addition, there are two feasible methods to increase lift force, one is to increase the energy density of the laser, and the other is to incorporate more photothermal particles in the LTMA.

2.4. 2D Self-Propellant Motions of LTMA

The LTMA can be driven by light–thermal effect for two reasons. First, as the LTMA is floating on the liquid–air interface and irradiated by a NIR laser beam, the laser-induced heat generates a local temperature that changes the surrounding liquid surface tension. Second, as the LTMA is heated by a NIR laser beam, the CA of pNIPAM/liquid will increase (temperature from 30 to 70 °C, CA from 20° to 30°) leading to an increasing system energy of pNIPAM/liquid in heated area. Therefore, the liquid surface tension and system energy difference cause the formation of the Marangoni flow

and the motion of LTMA. The moving direction of LTMA can be controlled by adjusting the light irradiation position (**Figure 4**a). In this way, the on-demand motion can be realized, including going straight, turning left, and turning right (Figure 4b–g; Videos S5–S7, Supporting Information). More programmable self-propellant motions of LTMA can be achieved by real-time manipulating the laser irradiation position. As a demonstration, the fish-like LTMA was fabricated and manipulated for obstacle avoidance in complex situations. As shown in Figure 4h,i, and Video S8, Supporting Information, the fish-like LTMA first floated up to the liquid surface and then moved from start position to end position along a W-shaped route and avoided obstacles successfully under the light drive. Moreover, the programmability of LTMA makes it possible to perform complex functional tasks. As demonstrations, the LTMA is used to finish the Sokoban game and push the cargo from the start location to the storage location (Figure S5 and Video S9, Supporting Information). Due to that the LTMA can float under the action of surface tension, it can be used to carry the objects. As shown in Figure S6 and Video S10, Supporting Information, a plastic ball was placed on the LTMA and transported from the start position to the end position. During the whole process in Figures S5 and S6, Supporting Information, the LTMA was under real-time manual control. Although it is still to be improved of the controllability of LTMA, we believe that fully automatic motion control functions and a predictable trajectory can be realized by using an automated real-time control system that integrates manipulation, detection, and feedback. In addition, the LTMA can be driven by the solar energy because it does not require much energy input to realize the motion. As shown in Figure S7 and Video S11, Supporting Information, the LTMA was driven under the irradiation of sunlight that was focused by a 5× magnifying glass. The use of clean energy for driving LTMA can expand the application fields of LTMA.

2.5. 3D Motions and Advanced Applications of LTMA

The LTMA can not only move on the liquid–air surface but also float/sink in the liquid, which enables the LTMA to play an important role in more advanced fields and applications. For example, LTMA can avoid obstacles on the liquid surface through another dimension by floating and sinking. As a demonstration of concept, we design an obstacle that blocks the liquid surface on the liquid–air interface (**Figure 5**a). However, LTMA is able to sink to the bottom of obstacle and cross it through the under-liquid route. As shown in Figure 5b, and Video S12, Supporting Information, the fish-like LTMA successfully overs the obstacle by sinking to the obstacle bottom, and then reached the end position. Furthermore, hydrogels are polymers with porous networks and can naturally absorb the surrounding chemical molecules, which makes the LTMA act as samplers. Hence, the LTMA can be used to absorb molecules from the target area and bring them back for further analysis. As a demonstration of concept, we drove LTMA to the target area for absorbing the target molecules (rhodamine 6G), and then manipulated it back for finishing the sampling
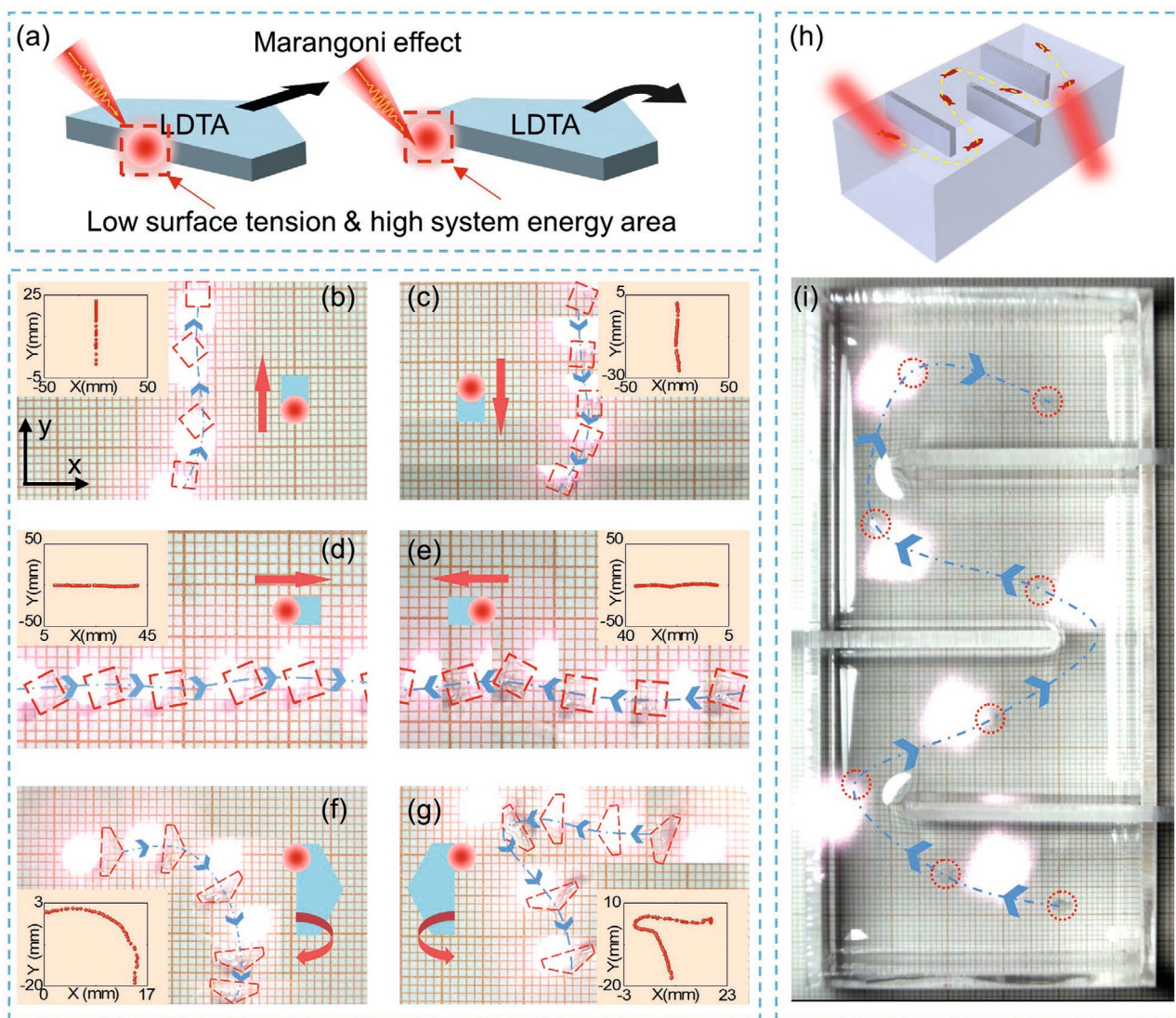
ADVANCED
SCIENCE NEWS

www.advancedsciencenews.com

ADVANCED
FUNCTIONAL
MATERIALS

www.afm-journal.de

Figure 4. The principle and control process of propulsion motion. a) Schematic illustration of directional motions induced by the Marangoni effect. Driven by laser beam, LTMA can finish self-propulsion motion such as b,c) moving down/up, d,e) moving left/right, and f,g) turning right/left. h,i) The schematic illustration and experimental results of conducting complex obstacle avoidance by LTMA.

process (Figure 5c; Video S13, Supporting Information). The LTMA was transparent before sampling while it absorbed rhodamine 6G molecules and became orange-red after sampling (Figure 5d). In the process of sampling, theoretically, the ability of LTMA to bring the signal back from the target area is not limited by distance, which is much more accurate and faster than detecting natural diffusion chemical signals. In the Video S13, Supporting Information, fluorescent also floats as the LTMA floats, which shows that the buoyancy flow not only raises the LTMA, but also raises the fluorescent molecules. In addition, by analyzing the RGB gray values of the collected LTMA optical photos, the color change of LTMA before and after sampling can be obtained quantitatively. As shown in Figure 5e,f, the peak value of the red channel has moved from 128 to 140, the gray value peak of the blue channel has moved from 101 to 44, and the peak of the green channel has moved from 130 to 105.

3. Conclusion

In conclusion, a transparent LTMA based on a nanoparticles-doped temperature-responsive hydrogel and a 3D manipulation strategy combining Marangoni effect with photothermal buoyancy flow has been reported. The LTMA can realize the programmable self-propellant motions on the liquid surface based on the Marangoni effect that relies on the surface tension difference, and can float/sink in the liquid by generating temperature-difference-induced photothermal buoyancy flow and absorbing liquid molecules. The dynamic generation process of buoyancy flow has been systemically investigated by the finite element simulations and experiments. The process of floating and sinking can be repeated as many times as required. The programmable controllability of LTMA makes it possible to perform complex tasks including finishing a Sokoban game and pushing/carrying the objects. Owing to that LTMA can move
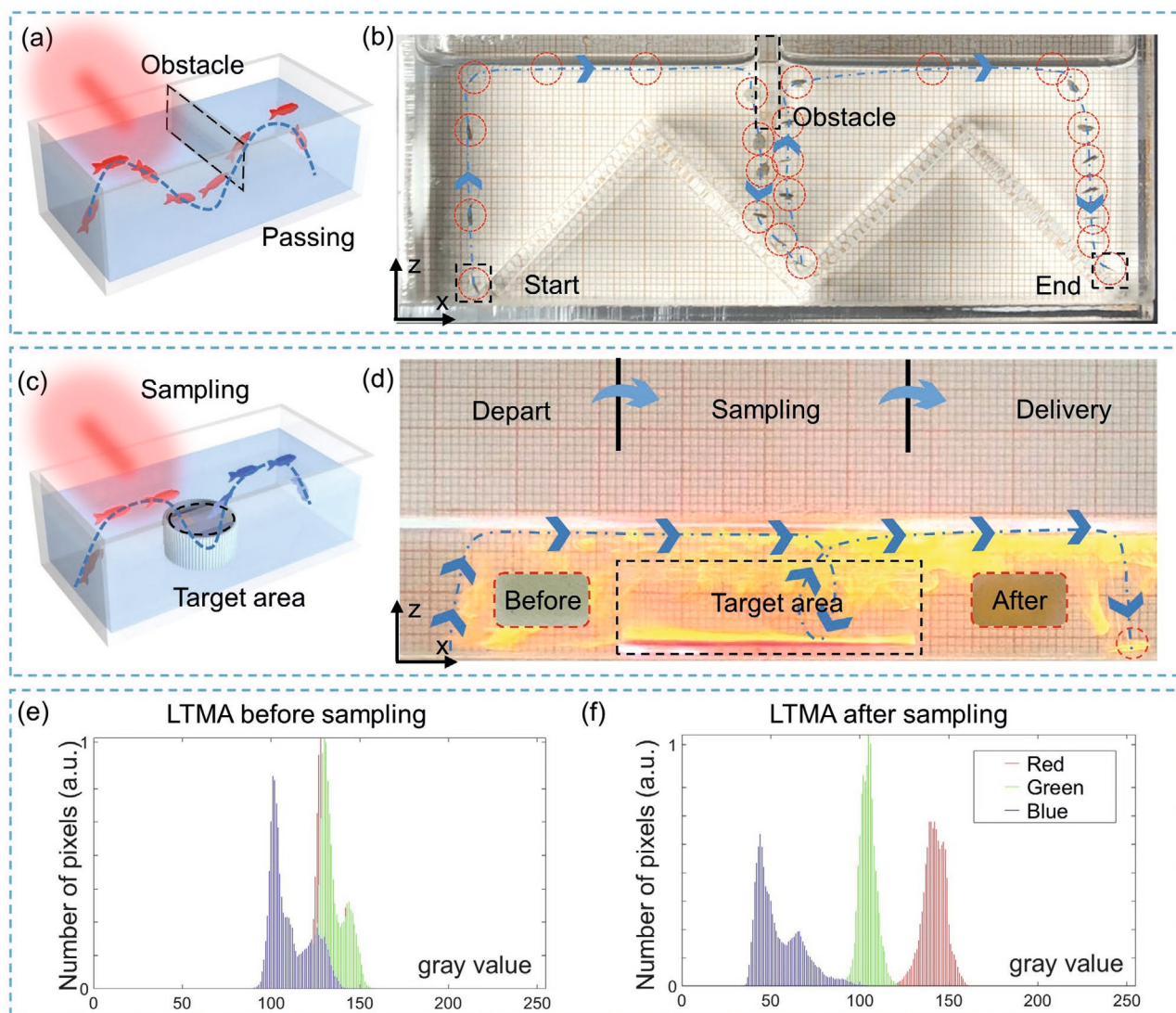
Figure 5. The applications of LTMA. a,b) LTMA can sink to the bottom of "iceberg" and pass over it. c,d) The processes of LTMA departing from the start position, sampling in the unknown area, and getting back for delivering the target-area signal. e,f) The RGB channel gray histogram of LTMA photographs before and after sampling, respectively.

three-dimensionally, it can be used in more advanced applications such as 3D obstacle avoidance that is difficult for the traditional MDA with 2D movement on the liquid surface. Besides, the LTMA mainly contains hydrogel that can naturally absorb the chemical molecules and can be used in remote sampling. This work extends the movements of traditional MDA from two dimensions to three dimensions by combining the photothermal buoyancy flow with Marangoni effect. The light-driven, transparent, three-dimensionally movable, and programmable actuator has promising prospects in the field of micromachines and intelligent systems.

4. Experimental Section

Materials: Copper bromide (CuBr$_2$, Sigma-Aldrich, 98%), sodium sulfide nonahydrate (Na$_2$S·9H$_2$O, Sigma-Aldrich, 98%), and sodium citrate (99%) were purchased from Sinopharm Chemical Reagent

Co. Other materials used in this study were *N*-isopropylacrylamide (Sigma-Aldrich, >97%), *N,N′*-methylenebis(acrylamide) (Sigma-Aldrich, >99%), lithium phenyl(2,4,6-trimethylbenzoyl)phosphinate (TCI Tokio Chemical Industry, >98%), fluorescein for fluorescence, and free acid (Sigma-Aldrich, 46955).

pNIPAM Resist: The resist was prepared dissolving 400 mg *N*-isopropylacrylamide, 40 mg *N,N′*-methylenebis(acrylamide), and 10 mg lithium phenyl(2,4,6-trimethylbenzoyl)phosphinate in 450 µL of ethylene glycol.

Synthesis of the CuS Nanoparticles: CuS nanoparticles were synthesized in mild conditions with a simple procedure. First, CuBr$_2$ (0.028 g) and sodium citrate (0.020 g) were added into deionized (DI) water (40.0 mL), and the mixture was stirred at room temperature for 1 h. After that, 50 µL Na$_2$S·9H$_2$O (0.024 g in 50 µL water) solution was added to the mixture with vigorous stirring and the solution was stirred for another 10 min at room temperature. Next, the mixture was transferred to a 90 °C water bath and reacted for 15 min to form the CuS nanoparticle. During the heating process, the color of mixture will turn to green. Finally, the CuS nanoparticle was obtained by cooling down the mixture to room temperature with an ice–water bath.

**ADVANCED
SCIENCE NEWS**

www.advancedsciencenews.com

**ADVANCED
FUNCTIONAL
MATERIALS**

www.afm-journal.de

Preparation of the LTMA: A total of 300 µL of DI water containing nanoparticles was taken and centrifuged at 1000 rpm for 5 min to remove the supernatant. The nanoparticles were taken out and added into 300 µL of pNIPAM resist. The volume ratio in this work refers to the ratio of the volume of the nanoparticle suspension to the volume of the hydrogel solution before centrifugation.

Laser Information: The laser used in this study was a handheld IR laser with center wavelength of 808 nm and energy density of 1 W cm^{-2}, model of ZLM2000AD808-34F.

Characterization: SEM images were obtained using a field emission scanning electron microscope (Sirion 200, FEI). The fluorescent images of the structures were taken by an inverted microscope with fluorescence (DMI 3000B, Leica). The CA tests were made using a CA100C contact-angle system (Innuo). UV–vis–NIR spectra were characterized by UV-3600 produced by Shimadzu. The surface temperatures of the LTMA were measured by a thermal infrared camera (VarioCAM hr head 680, InfraTec).

Supporting Information

Supporting Information is available from the Wiley Online Library or from the author.

Conflict of Interest

The authors declare no conflict of interest.

Keywords

buoyancy flow, hydrogels, light-driven actuators, Marangoni effect

[1] a) B. Han, Y.-L. Zhang, Q.-D. Chen, H.-B. Sun, *Adv. Funct. Mater.* **2018**, *28*, 1802235; b) O. M. Wani, H. Zeng, A. Priimagi, *Nat. Commun.* **2017**, *8*, 15546.

[2] W. T. Jiang, D. Niu, H. Z. Liu, C. H. Wang, T. T. Zhao, L. Yin, Y. S. Shi, B. D. Chen, Y. C. Ding, B. H. Lu, *Adv. Funct. Mater.* **2014**, *24*, 7598.

[3] a) M. Amjadi, M. Sitti, *ACS Nano* **2016**, *10*, 10202; b) Y. L. Zhang, Y. Q. Liu, D. D. Han, J. N. Ma, D. Wang, X. B. Li, H. B. Sun, *Adv. Mater.* **2019**, *31*, 1901585; c) M. Salehizadeh, O. Onaizah, E. Diller, *Sci. Rob.* **2019**, *4*, eaav4494.

[4] a) S. Palagi, A. G. Mark, S. Y. Reigh, K. Melde, T. Qiu, H. Zeng, C. Parmeggiani, D. Martella, A. Sanchez-Castillo, N. Kapernaum, F. Giesselmann, D. S. Wiersma, E. Lauga, P. Fischer, *Nat. Mater.* **2016**, *15*, 647; b) L. Dong, Y. Zhao, *Mater. Chem. Front.* **2018**, *2*, 1932; c) S. Ma, X. Li, S. Huang, J. Hu, H. Yu, *Angew. Chem., Int. Ed. Engl.* **2019**, *58*, 2655; d) Z. Lao, Y. Zheng, Y. Dai, Y. Hu, J. Ni, Z. Cai, Z. J. Smith, J. Li, L. Zhang, D. Wu, J. Chu, *Adv. Funct. Mater.* **2020**, *30*, 1909467; e) S. Zhu, Y. Bian, T. Wu, C. Chen, Y. Jiao, Z. Jiang, Z. Huang, E. Li, J. Li, J. Chu, Y. Hu, D. Wu, L. Jiang, *Nano Lett.* **2020**, *20*, 5513; f) Y. Hu, Z. Wang, X. Wang, S. Ji, C. Zhang, J. Li, W. Zhu, D. Wu, J. Chu, *Light: Sci. Appl.* **2020**, *9*, 119; g) D. Wu, Z. Zhang, Y. Zhang, Y. Jiao, S. Jiang, H. Wu, C. Li, C. Zhang, J. Li, Y. Hu, G. Li, J. Chu, L. Jiang, *Adv. Mater.* **2020**, *32*, 2005039; h) Y. Hu, H. Yuan, S. Liu, J. Ni, Z. Lao, C. Xin, D. Pan, Y. Zhang, W. Zhu, J. Li, D. Wu, J. Chu, *Adv. Mater.* **2020**, *32*, 2002356.

[5] a) D. D. Han, Y. L. Zhang, J. N. Ma, Y. Q. Liu, B. Han, H. B. Sun, *Adv. Mater.* **2016**, *28*, 8328; b) H. Lim, T. Park, J. Na, C. Park, B. Kim, E. Kim, *NPG Asia Mater.* **2017**, *9*, e399; c) X. Pang, J. A. Lv, C. Zhu, L. Qin, Y. Yu, *Adv. Mater.* **2019**, *31*, 1904224; d) T. Zhang, H. Chang, Y. Wu, P. Xiao, N. Yi, Y. Lu, Y. Ma, Y. Huang, K. Zhao, X.-Q. Yan, Z.-B. Liu, J.-G. Tian, Y. Chen, *Nat. Photonics* **2015**, *9*, 471; e) H. Xin, B. Li, *Light: Sci. Appl.* **2014**, *3*, e205.

[6] C.-H. Zhu, Y. Lu, J. Peng, J.-F. Chen, S.-H. Yu, *Adv. Funct. Mater.* **2012**, *22*, 4017.

[7] M. Liao, H. Sun, X. Tao, X. Xu, Z. Li, X. Fu, S. Xie, L. Ye, Y. Zhang, B. Wang, X. Sun, H. Peng, *ACS Appl. Mater. Interfaces* **2018**, *10*, 26765.

[8] a) R. L. Yang, Y. J. Zhu, D. D. Qin, Z. C. Xiong, *ACS Appl. Mater. Interfaces* **2019**, *12*, 1339; b) R.-L. Yang, Y.-J. Zhu, F.-F. Chen, D.-D. Qin, Z.-C. Xiong, *ACS Sustainable Chem. Eng.* **2019**, *7*, 13226; c) X. Su, H. Li, X. Lai, Z. Yang, Z. Chen, W. Wu, X. Zeng, *J. Mater. Chem. A* **2018**, *6*, 16910.

[9] D. Okawa, S. J. Pastine, A. Zettl, J. M. Frechet, *J. Am. Chem. Soc.* **2009**, *131*, 5396.

[10] M. Gugliotti, M. S. Baptista, M. J. Politi, *J. Chem. Educ.* **2004**, *81*, 824.

[11] C. Maggi, F. Saglimbeni, M. Dipalo, F. De Angelis, R. Di Leonardo, *Nat. Commun.* **2015**, *6*, 7855.

[12] W. Wang, Y.-Q. Liu, Y. Liu, B. Han, H. Wang, D.-D. Han, J.-N. Wang, Y.-L. Zhang, H.-B. Sun, *Adv. Funct. Mater.* **2017**, *27*, 1702946.

[13] D. G. de Vahl, J. Int, N. Meth, *Fluids* **1983**, *3*, 249.

[14] M. Hippler, E. Blasco, J. Qu, M. Tanaka, C. Barner-Kowollik, M. Wegener, M. Bastmeyer, *Nat. Commun.* **2019**, *10*, 232.

[15] a) C. Ma, X. Le, X. Tang, J. He, P. Xiao, J. Zheng, H. Xiao, W. Lu, J. Zhang, Y. Huang, T. Chen, *Adv. Funct. Mater.* **2016**, *26*, 8670; b) C. Ma, W. Lu, X. Yang, J. He, X. Le, L. Wang, J. Zhang, M. J. Serpe, Y. Huang, T. Chen, *Adv. Funct. Mater.* **2018**, *28*, 1704568.

[16] a) T. Y. Huang, H. W. Huang, D. D. Jin, Q. Y. Chen, J. Y. Huang, L. Zhang, H. L. Duan, *Sci. Adv.* **2020**, *6*, eaav8219; b) S. Fusco, H. W. Huang, K. E. Peyer, C. Peters, M. Haberli, A. Ulbers, A. Spyrogianni, E. Pellicer, J. Sort, S. E. Pratsinis, B. J. Nelson, M. S. Sakar, S. Pane, *ACS Appl. Mater. Interfaces* **2015**, *7*, 6803; c) Y. Hu, Z. Wang, D. Jin, C. Zhang, R. Sun, Z. Li, K. Hu, J. Ni, Z. Cai, D. Pan, X. Wang, W. Zhu, J. Li, D. Wu, L. Zhang, J. Chu, *Adv. Funct. Mater.* **2019**, *30*, 1907377.

[17] a) G. Chen, B. Ma, Y. Wang, R. Xie, C. Li, K. Dou, S. Gong, *ACS Appl. Mater. Interfaces* **2017**, *9*, 41700; d) X. Nie, L. Xia, H. L. Wang, G. Chen, B. Wu, T. Y. Zeng, C. Y. Hong, L. H. Wang, Y. Z. You, *ACS Appl. Mater. Interfaces* **2019**, *11*, 31735.

[18] R. Pelton, *J. Colloid Interface Sci.* **2010**, *348*, 673.